AGU PUBLICATIONS

JGR

Journal of Geophysical Research: Earth Surface

RESEARCH ARTICLE

10.1002/2014JF003341

Key Points:
- Short-lived closure events were not initiated by perturbations in ice velocity
- Velocity fluctuations and morainal geometry control glacier terminus position
- Closure of the channel at Gilbert Point is likely to occur this century

Supporting Information:
- Table S1
- Table S2
- Figure S1

Correspondence to:
L. A. Stearns,
stearns@ku.edu

Citation:
Stearns, L. A., G. S. Hamilton, C. J. van der Veen, D. C. Finnegan, S. O'Neel, J. B. Scheick, and D. E. Lawson (2015), Glaciological and marine geological controls on terminus dynamics of Hubbard Glacier, southeast Alaska, *J. Geophys. Res. Earth Surf.*, *120*, 1065–1081, doi:10.1002/2014JF003341.

Received 15 SEP 2014
Accepted 21 APR 2015
Accepted article online 30 MAR 2015
Published online 25 JUN 2015

Glaciological and marine geological controls on terminus dynamics of Hubbard Glacier, southeast Alaska

L. A. Stearns[1], G. S. Hamilton[2], C. J. van der Veen[3], D. C. Finnegan[4], S. O'Neel[5], J. B. Scheick[2], and D. E. Lawson[4]

[1]Department of Geology, University of Kansas, Lawrence, Kansas, USA, [2]School of Earth and Climate Sciences, University of Maine, Orono, Maine, USA, [3]Department of Geography, University of Kansas, Lawrence, Kansas, USA, [4]USACE Cold Regions Research and Engineering Laboratory, Hanover, New Hampshire, USA, [5]Alaska Science Center, USGS, Anchorage, Alaska, USA

Abstract Hubbard Glacier, located in southeast Alaska, is the world's largest nonpolar tidewater glacier. It has been steadily advancing since it was first mapped in 1895; occasionally, the advance creates an ice or sediment dam that blocks a tributary fjord (Russell Fiord). The sustained advance raises the probability of long-term closure in the near future, which will strongly impact the ecosystem of Russell Fiord and the nearby community of Yakutat. Here, we examine a 43 year record of flow speeds and terminus position to understand the large-scale dynamics of Hubbard Glacier. Our long-term record shows that the rate of terminus advance has increased slightly since 1895, with the exception of a slowed advance between approximately 1972 and 1984. The short-lived closure events in 1986 and 2002 were not initiated by perturbations in ice velocity or environmental forcings but were likely due to fluctuations in sedimentation patterns at the terminus. This study points to the significance of a coupled system where short-term velocity fluctuations and morainal shoal development control tidewater glacier terminus position.

1. Background

Large uncertainties in estimating local and global impacts of changing glaciers worldwide, including those draining polar ice sheets, stem from our limited understanding of glaciers that directly interact with the ocean (tidewater glaciers). This behavior includes both rapid retreat and advances that may be nonsynchronous with climate trends and other glaciers in the region [e.g., *Arendt et al.*, 2006; *Larsen et al.*, 2007; *Meier et al.*, 2007]. While the majority of tidewater glaciers in Greenland, Antarctica, and Alaska are retreating, some are advancing. In most cases, advancing glaciers neighbor retreating ones, highlighting the complexity of controls on terminus behavior [e.g., *Post et al.*, 2011]. Here we investigate the glaciological and marine controls on terminus dynamics of Hubbard Glacier, the largest nonpolar tidewater glacier in the world.

Hubbard Glacier, located in southeast Alaska, has an intriguing history; it retreated during the Little Ice Age when neighboring glaciers advanced and is currently advancing while neighboring glaciers recede [*Barclay et al.*, 2001; *Trabant et al.*, 2003; *McNabb and Hock*, 2014]. While Hubbard Glacier may behave independently of climate trends [*Trabant et al.*, 1991], its flow dynamics suggest a strong correlation with seasonal forcings [*Motyka and Truffer*, 2007; *Ritchie et al.*, 2008].

The catchment of Hubbard Glacier covers an area of ~3900 km^2 and extends from Mount Logan at 5959 m to sea level in Disenchantment Bay (Figure 1). The glacier's hypsometry — with 95% of its surface area above the equilibrium line altitude (ELA) — dampens its sensitivity to short-term climate variability [*Motyka and Truffer*, 2007]. Over long timescales, its behavior is typical of tidewater glaciers—slow advances take 1—1.5 kyr, and are punctuated by rapid retreats [e.g., *Post*, 1975; *Trabant et al.*, 1991; *Barclay et al.*, 2001]. Three major advances in the Holocene brought ice well into Disenchantment Bay [*Barclay et al.*, 2001]. During the last and largest advance (ca. C.E. 1000) [*Barclay et al.*, 2001], ice reached the mouth of Yakutat Bay, ~65 km beyond its current position. Retreat was underway by 1308 A.D., and by 1791 the terminus was located upstream of the current position [*Barclay et al.*, 2001]. This large terminus retreat significantly modified the accumulation area ratio (AAR) and subsequently the glacier's surface mass balance. Hubbard Glacier's steady advance is sustained by the current AAR of 0.95 (Figure 1), coupled with high accumulation rates (~2 mwe, based on measurements of average surface mass balance in the accumulation area of neighboring Variegated Glacier

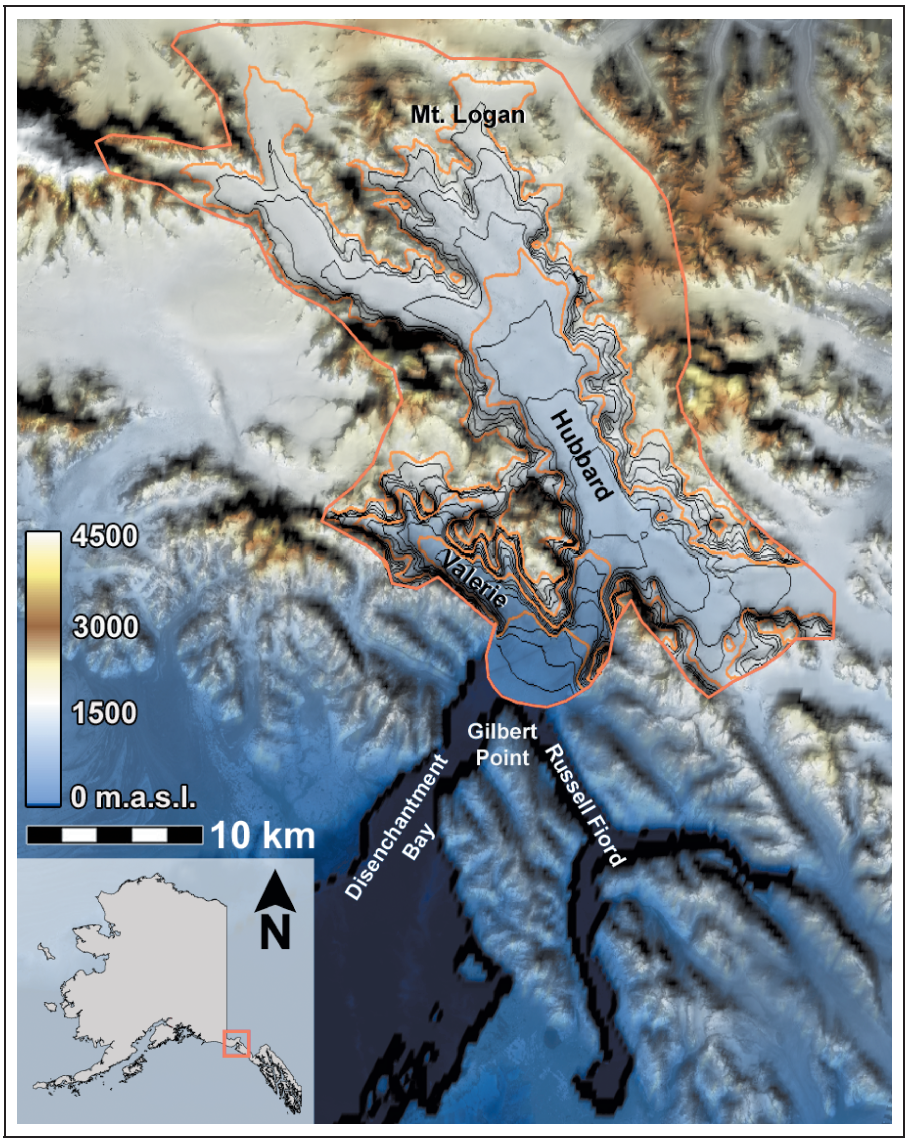

Figure 1. Hubbard Glacier's catchment area. Elevation contours mark every 100 m with orange lines indicating 500 m intervals. The equilibrium line altitude (ELA) is at ~1000 m [*Trabant et al.*, 2003]. Valerie Glacier flows into the western side of Hubbard Glacier's terminal lobe; Gilbert Point is at the apex of the peninsula that divides Russell Fiord from Disenchantment Bay. Elevation data are from the Shuttle Radar Topography Mission (SRTM) [*USGS*, 2006], and the background Landsat image is from 9 August 2003 [*NASA Landsat Program*, 2003].

[*Trabant et al.*, 1991]) [*Trabant et al.*, 2003]. The advance is likely to continue unless the AAR is reduced to 0.7, which would require a 1000 m increase in the ELA [*Trabant et al.*, 2003]. Such a large shift is unlikely to occur in the near future.

The trunk of Hubbard Glacier funnels through a narrow (~2.5 km) valley in the St. Elias Mountain range. At the mouth of the valley, the glacier spreads into a ~14 km wide terminal lobe, which ends at the head of Disenchantment Bay and the mouth of Russell Fiord (Figure 1). *Trabant et al.* [1991] estimate that approximately 95% of the mass flux from the accumulation area is lost by calving, 4% is melted at the surface, and 1% goes into growing the terminal lobe. Ice thickness data from radio-echo soundings near the centerline suggest that the terminal lobe lies within an overdeepened basin ~400 m below sea level [*Trabant et al.*, 1991, 2003; *Rignot et al.*, 2013]. The ice cliff at the front of the terminal lobe is grounded and ~200 m thick [*Trabant et al.*, 1991], with 60–100 m above sea level. Repeat bathymetry data reveal that Hubbard Glacier advances at the same rate as a morainal bank, on which it is persistently grounded [*Goff et al.*, 2012].

Table 1. Errors Associated With Tracing Quantifying the Terminus Area Using Imagery of Different Resolutions[a]

	Landsat MSS	Landsat TM	Landsat ETM+	ERS 1/2
Temporal range	1979–1993	1984–present	1999–present	1991/1995–2000/2011
Resolution (m)	60	30	15	12.5–50
Resolution errors (km^2)	0.42	0.32	0.20	0.24–0.51
Digitizing errors (km^2)	0.20	0.15	0.10	0.04–0.07
Total errors (km^2)	0.46	0.35	0.22	0.24–0.52

[a]The resolution uncertainty reflects the difference in the average area traced for a specific resolution, as compared to a 60 cm resolution QuickBird image. Digitizing errors show the variation in the manual tracing process.

Of particular interest to local communities is the behavior of Hubbard Glacier's terminal lobe, which flows around Gilbert Point into Disenchantment Bay to the west and Russell Fiord to the east (Figure 1). A narrow marine channel along Gilbert Point connects Disenchantment Bay and Russell Fiord. Historically, ice (1986) and sediment (2002) dams temporarily blocked this channel, causing water levels in Russell Fiord to rise 25.5 m and 18.6 m, respectively [*Motyka and Truffer*, 2007]. Both dams failed catastrophically after 2–4 months. However, the sustained advance of Hubbard Glacier will likely create a permanent ice dam at Gilbert Point, close the tidal channel that drains Russell Fiord into Disenchantment Bay, and transform the large, paraglacial fjord system into a 64 km long proglacial lake. Changes in water chemistry, sediment concentration, stream gradients, and circulation as a result of impoundment will potentially cause major ecological changes in the Russell Fiord watershed. This new lake would drain through the Situk River, where it may have major socioeconomic consequences for local populations due to the impacts on regional fishing [*Daly et al.*, 2011].

Since the last closure event in 2002, the gap between the terminus and Gilbert Point has decreased to less than 200 m on several occasions [*Finnegan et al.*, 2010]. However, the controls on tidewater glacier behavior are numerous and complex and have thus prevented accurate predictions of future closure events [e.g., *Trabant et al.*, 1991]. Long-term and continuous records are essential to understanding a glacier's response to different forcings, yet such records are rare. Here we examine a 43 year record of flow speeds, terminus position, climate, and oceanographic data to understand the large-scale dynamics of Hubbard Glacier and how it responds to environmental forcings. We are particularly interested in understanding the factors that control terminus position as well as those leading to the sustained advance of the terminus and the likely closure of Russell Fiord.

2. Methods

2.1. Terminus Position

Our record of terminus positions is based on optical images from the Landsat archive and radar images from the ERS 1/2 satellites (© ESA (2011)), the latter of which are used to bridge data gaps in Landsat caused by bad weather or solar illumination (Table S1 in the supporting information). Each image is reprojected into a common coordinate system (UTM 7, WGS-84 ellipsoid) and coregistered to a Landsat Enhanced Thematic Mapper (ETM+) image from 13 July 2002. Several early generation Landsat images (Landsat MultiSpectral Scanner (MSS) and Thematic Mapper (TM)) had poor georeferencing and had to be manually coregistered to our ETM+ master image. The resolution of the Landsat images depends on the sensor generation and varies from 15 to 60 m (Table 1). We apply a crisp filter to the 60 m resolution images to make the terminus edge more distinct. The ERS 1/2 images have a resolution of either 50 m (standard images) or 12.5 m (precision images); we use the precision images where available. A panchromatic QuickBird image from 18 September 2007, with a resolution of 60 cm, is used to calculate resolution uncertainties. Our record of terminus positions builds on previous work done by *Ritchie et al.* [2008] (whose record is from 1992–2004) and *McNabb and Hock* [2014] (who use only the Landsat archive for their 1972–2012 record).

We extend our record beyond the Landsat archive (1972) by digitizing terminus data from *Trabant et al.* [1991, Figure 11]. *Trabant et al.* [1991] use terminus data from the 1895 International Boundary Commission map and aerial photographs acquired in 1948 and 1962. We verify the 1948 and 1962 terminus positions by using georeferenced U.S. Geological Survey (USGS) topographic maps from 1951 and 1961, following the methodology

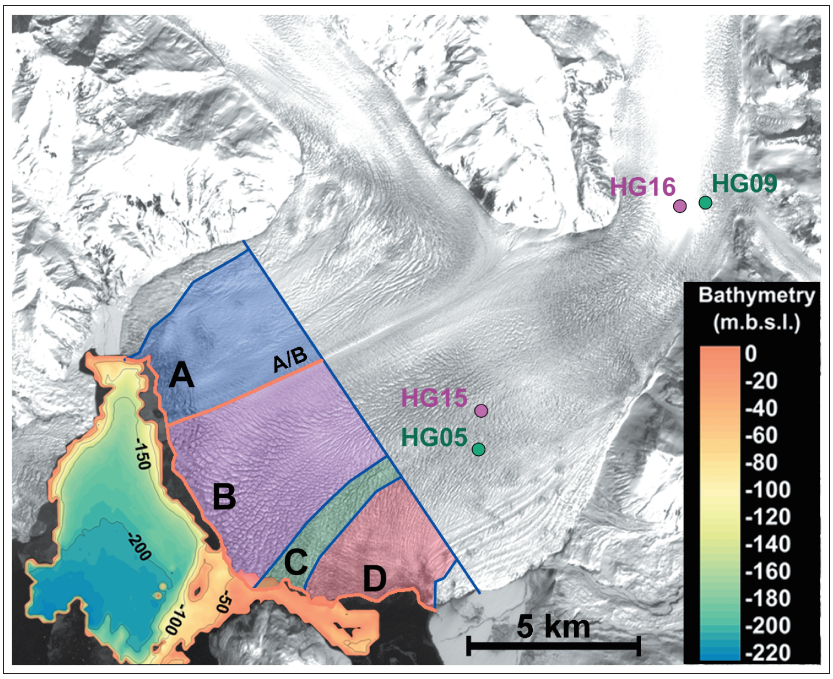

Figure 2. Sections delineating the terminus area of Hubbard Glacier (modified from *Ritchie et al.* [2008]), overlain on a Landsat ETM+ image from 24 April 2002 [*NASA Landsat Program*, 2002]. Fixed boundaries are blue; dynamic boundaries are red (including medial moraine A/B). Locations of GPS receivers deployed in May (HG05, HG09) and September (HG15, HG16) 2010 are shown as circles. Seafloor bathymetry (meters below sea level) adjacent to Hubbard Glacier's terminus was obtained during 1999 [*NOAA*, 2000] and 2008 [*Finnegan et al.*, 2010] surveys. Note that terminus advance since the 1999 survey explains the overlapping data sets near Gilbert Point.

of *McNabb and Hock* [2014]. The 1951 USGS map is based on the collection of aerial photographs from 1948; the terminus position in the 1961 USGS map compares well with the position noted by *Trabant et al.* [1991] for 1962.

A convenient way to analyze the asymmetric terminus advance of Hubbard Glacier is to divide the terminal lobe into distinct regions, similar to *Ritchie et al.* [2008, Figure 2]. We divide the lobe into four regions (Figure 2) to investigate patterns of advance for different flow regimes of the terminus. Region A contains ice originating from Valerie Glacier; Region B consists of Hubbard Glacier ice draining into Disenchantment Bay; Region C is Hubbard Glacier ice flowing toward Gilbert Point; Region D is Hubbard Glacier ice that drains into Russell Fiord. All lateral boundaries are fixed to isolate terminus advance (as opposed to changes in glacier width), except for the medial moraine A/B which migrates based on the dynamic behavior of Valerie and Hubbard glaciers. The area in each terminus region is derived from satellite imagery, following the technique described by *Moon and Joughin* [2008] and *Schild and Hamilton* [2013]. This technique differs from previous Hubbard studies where the terminus position (as opposed to area) is determined as the distance from a fixed point [e.g., *Krimmel and Sikonia*, 1986; *Mayo*, 1989; *Trabant et al.*, 2003].

Uncertainties in the terminus area derive from coregistration and manual digitizing errors. To minimize coregistration errors, we stack sequential images and terminus vector files, tracing identifiable features (and the terminus position) between image pairs to ensure there is no offset of static features (and only reasonable movement of the terminus position). Digitizing errors are dependent on the image resolution and the repeatability of the operator. The uncertainty associated with resolution is quantified by calculating the terminus area from two sensors (MSS versus TM, TM versus ETM+, ERS 1/2 versus ETM+) during the same time period (all image sequences have overlapping acquisition periods). The results are cumulative, so that the standard deviation (Table 1) reports the area difference between each resolution and a 60 cm QuickBird image. We quantify the repeatability of the digitizing process by tracing the terminus area from the same image 10 times and determining the standard deviation [after *Schild and Hamilton*, 2013].

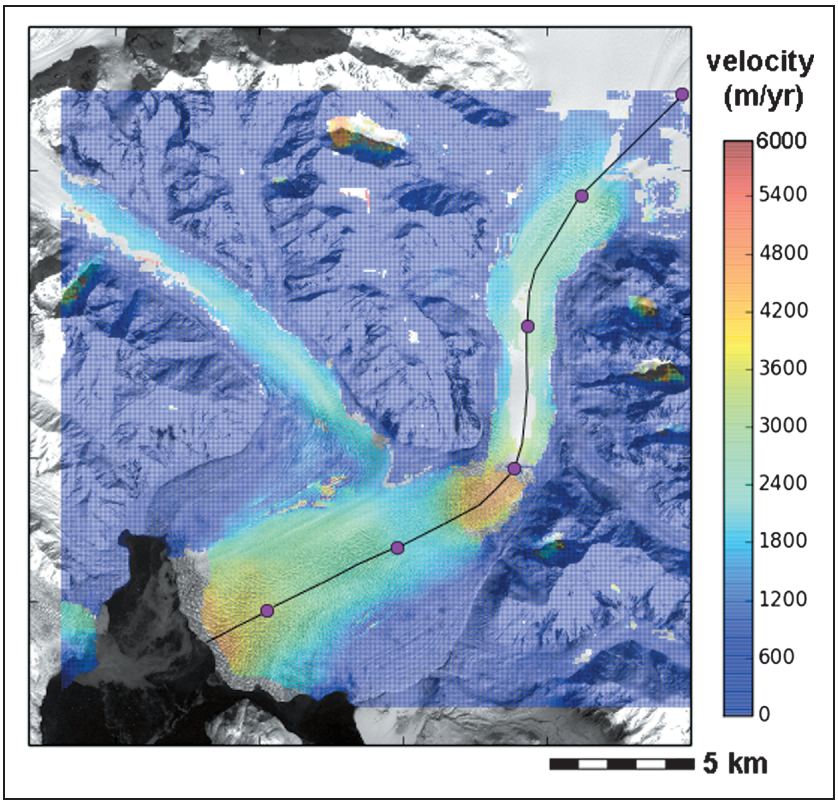

Figure 3. Ice velocity derived from two Landsat images acquired on 8 and 24 April 2002, overlain on a Landsat ETM+ image from 8 April 2002 [*NASA Landsat Program*, 2002]. Centerline velocities for different epochs are derived along the black line, with circles every 5 km (results shown in Figure 7.

2.2. Ice Velocity

We estimate ice velocity using both satellite remote sensing techniques and ground-based Global Positioning System (GPS) receivers. Remote sensing velocities are derived from automatic tracking of surface features on sequential images using a cross-correlation technique implemented in the IMCORR software package [*Scambos et al.*, 1992] (Figures 3 and S1). The measured displacements of surface features have several sources of uncertainty originating from image coregistration. Landsat scenes are orthorectified using a digital elevation model (DEM) derived from an Advanced Spaceborne Thermal Emission and Reflection Radiometer (ASTER) image acquired on 20 May 2003. We assign a coregistration error of one pixel for each image after *Stearns and Jiskoot* [2014]. Poor spatial resolution and infrequent image acquisition prevent us from tracking features on the 60 m Landsat MSS scenes. Overall, resampling errors during orthoprojection translate to positional errors at the subpixel level (<15 m for Landsat ETM+ and <30 m for Landsat TM). Uncertainties associated with the image cross-correlation technique are also subpixel in scale [*Scambos et al.*, 1992; *Stearns and Jiskoot*, 2014] and correlations with uncertainties larger than one pixel are discarded. Velocity errors scale with the time separation of the image pairs (Table S2). The feature tracking technique produces dense coverage over heavily crevassed areas of the glacier but does not produce many matches in regions with minimal or no crevassing, corresponding roughly to the central parts of the glacier trunk. We use nearest-neighbor interpolation to grid the velocity components onto 150 m grids.

In 2010, dual-frequency GPS receivers deployed on Hubbard Glacier collected position measurements at a sampling rate of 5 s from 18–24 May to 18–22 September (Figure 2). We use the GIPSY software package to process GPS data and estimate ice velocity [after *Lichten and Border*, 1987], which we subsequently use to evaluate the feature tracking technique. May GPS results are compared to velocities derived from 17 May and 9 June 2010 image pairs; September GPS results are compared to velocities derived from 6 and 22 September image pairs.

Further insight into spatial and temporal changes in ice flow can be obtained by estimating surface strain rates from the satellite-derived velocities. Strain rates are initially determined in the original orientation of

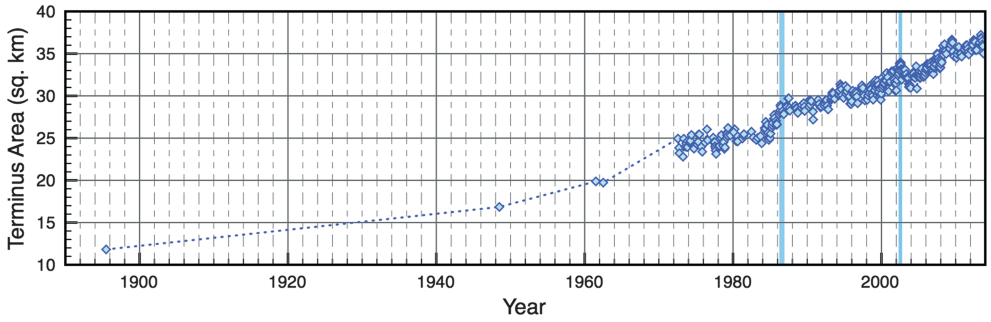

Figure 4. Hubbard Glacier's total terminus area, from 1895 to 2014. Blue vertical bars indicate known periods when Hubbard Glacier reached Gilbert Point, damming Russell Fiord.

the grid ($\dot{\varepsilon}_{ij}$). Subsequently, the strain rate tensor at each grid cell is rotated ($\dot{\varepsilon}'_{ij}$) so that the x axis is oriented downflow and the y axis is acrossflow. The flow direction (ϕ) is determined for each grid cell, and strain rate tensor components are rotated following [*Jaeger and Cook*, 1976]:

$$\begin{aligned}\dot{\varepsilon}'_{xx} &= \dot{\varepsilon}_{xx}(\cos\phi)^2 + \dot{\varepsilon}_{yy}(\sin\phi)^2 + 2\,\dot{\varepsilon}_{xy}\sin\phi\cos\phi \\ \dot{\varepsilon}'_{yy} &= \dot{\varepsilon}_{xx}(\sin\phi)^2 + \dot{\varepsilon}_{yy}(\cos\phi)^2 - 2\,\dot{\varepsilon}_{xy}\sin\phi\cos\phi \\ \dot{\varepsilon}'_{xy} &= (-\dot{\varepsilon}_{xx} + \dot{\varepsilon}_{yy})(\sin\phi\cos\phi) + \dot{\varepsilon}_{xy}\,[2(\cos\phi)^2 - 1].\end{aligned} \tag{1}$$

These strain rate components describe longitudinal stretching, lateral spreading, and shearing at the glacier surface, respectively. Uncertainties originate from the errors in surface velocity during each epoch and are carried through the strain rate calculations [*Wuite*, 2006] assuming that the errors are random. The strain rate errors are 0.5 year^{-1}, on average (Table S2).

2.3. Climate

We obtain precipitation and air temperature records from the Global Historical Climatology Network (GHCN) version 2 (adjusted) data set, compiled by the NOAA National Climatic Data Center. Weather station data comes from the town of Yakutat, roughly 50 km from Hubbard Glacier (WMO station code: 70361, at 59.52°N, 139.67°W, 4 m asl (above sea level)), which has continuous data from 1917 to present. We explore the relationship between these climate indices and the Pacific Decadal Oscillation (PDO) using data from the National Climatic Data Center (available at: http://www.ncdc.noaa.gov/teleconnections/pdo/).

Since there are no long-term moorings in Disenchantment Bay, we rely on two different data sets to investigate how ocean conditions adjacent to Hubbard Glacier may have changed during the period of our record. A shallow sill (only 15 m deep in places) at the mouth of Yakutat Bay prohibits deep ocean water from entering Disenchantment Bay [*Wright*, 1972]. As a result, we assume the water adjacent to the glacier terminus is physically similar to the surface waters of Yakutat Bay. Thus, we use two data sets that record sea surface temperatures (SSTs) and temperatures of the upper water column. Sea surface temperatures are taken from the NOAA Reynolds version 2 data set, which provides weekly, 1° grids from a combination of in situ measurements, satellite-derived SSTs, and SSTs simulated based on sea ice cover. We extract the SSTs over an area including all of Yakutat Bay and ~20 km into the Gulf of Alaska (59.2–60.1°N, 139.5–140.2°W) (similar to *Ritchie et al.* [2008]). We also use data from an oceanographic station near Seward, Alaska, that measures salinity and temperature of the Alaska Current (from the surface to a depth of 250 m). The Alaska Current is the predominant upper level water along southeast coastal Alaska and flows past Yakutat Bay. Data are publicly available at http://www.ims.uaf.edu/gak1/.

3. Results

3.1. Terminus Area

Hubbard Glacier has been steadily advancing since its terminus was first mapped in 1895 (Figure 4). While the record is scarce prior to 1972, measurements derived from aerial photographs suggest that advance rates have increased over time, consistent with conclusions by *Trabant et al.* [1991]. Our results also show that advance rates slowed for a brief time between 1972 and 1984 (Figure 4). The rate of advance is calculated by dividing the area change between two time periods by the width of the region and the time separation. Between

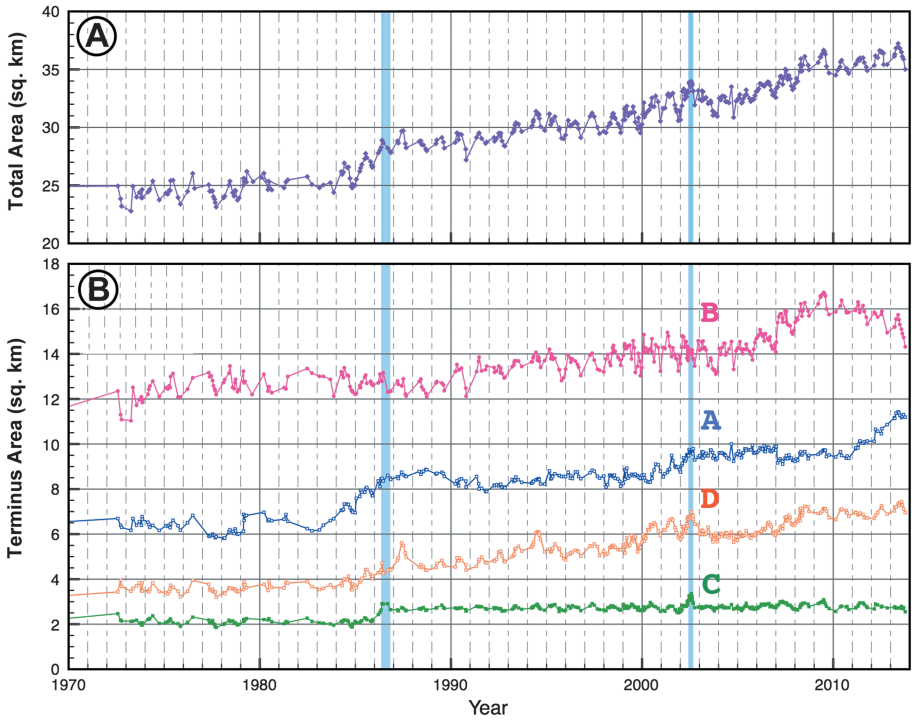

Figure 5. Time series of terminus area for (a) the entire terminus and (b) for regions A–D, delineated in Figure 2. Blue vertical bars indicate periods when Hubbard Glacier reached Gilbert Point, damming Russell Fiord.

July 1972 and July 1984, the annual width-averaged rate of advance was 13 m yr^{-1}. Rates before (1961–1972: 36 m yr^{-1}) and after (1984–2014: 35 m yr^{-1}) this time period were more than twice as high. These high rates are similar to those found by *Ritchie et al.* [2008] (35 m yr^{-1} from 1992 to 2006) and *McNabb and Hock* [2014] (34 m yr^{-1} from 1961 to 2012). Prior to 1961, advance rates were between 9 m yr^{-1} (1895–1948) and 23 m yr^{-1} (1948–1961).

Figure 5 shows that patterns of advance are not distributed evenly across the terminus [*Ritchie et al.*, 2008]. Instead, each region exhibits a unique behavior. Region A (originating from Valerie Glacier) undergoes large, periodic advances. Region B (draining into Disenchantment Bay) has the largest seasonal variability but a relatively small overall advance. Region C (adjacent to Gilbert Point) underwent large advances around closure years but its overall advance is minor. Region D (draining into Russell Fiord) has a relatively steady advance that is punctuated, roughly every 7 years, by a year of increased advance.

Regions A and B share a medial moraine; in many cases these two areas exhibit out-of-phase behavior over decadal timescales, reflecting moraine migration. Moraine migration is likely caused by fluctuations in ice flux from Valerie and Hubbard glaciers. Valerie Glacier exhibits surge-like behavior [*Mayo*, 1989] on short timescales, which causes moraine displacement [*Ritchie et al.*, 2008]. The large expansion of Region A between 1984 and 1988 resulted from a combination of terminus advance (by ~500 m) and moraine shift to the east (by ~400 m at the terminus) (Figure 5). The area of Region B decreased slightly during this time, but did not offset the growth of Region A, indicating that terminus advance also occurred in this region. The expansion of Region B at the expense of Region A between 2005 and 2009 was caused by a shift of the medial moraine to the west by ~220 m and an advance of both regions by ~400 m. Between 2010 and 2013, the medial moraine migrated back to the southeast, resulting in an area decrease of Region B and increase of Region A; Region A also advanced slightly more than Region B did during this time period.

Medial moraine migration is coincident with terminus advance and is typically short-lived—the expansion of Region A (from 1984 to 1988 and, more subtly, from 2000 to 2006) lasted 4–6 years and may have been initiated by periodic weak surges of Valerie Glacier [*Ritchie et al.*, 2008]. Since the length of the medial moraine is ~9 km and the annual average speed of the terminal lobe is ~2000 m yr^{-1}, it takes approximately 4.5 years for a perturbation at the origin of the medial moraine (where Valerie joins Hubbard) to propagate to the terminus.

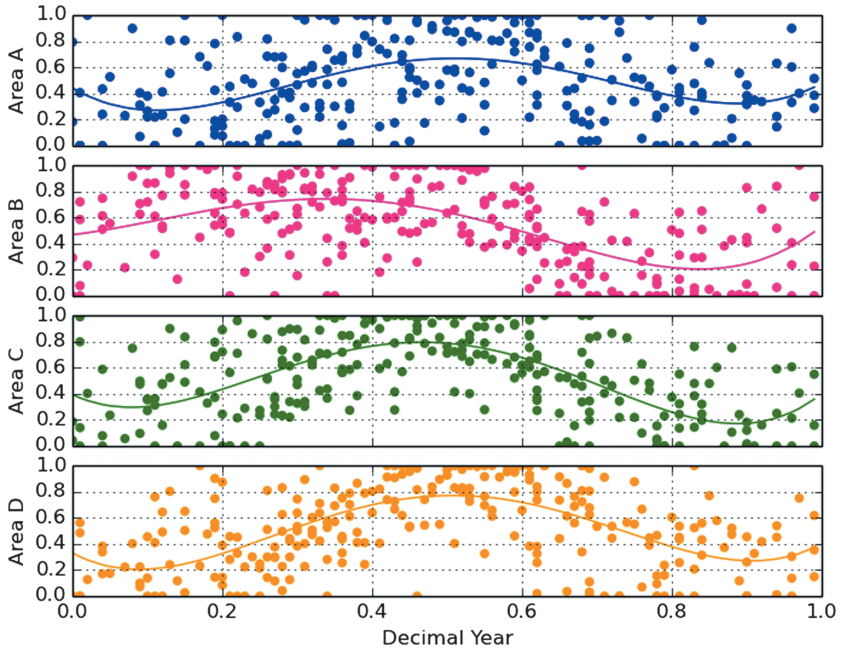

Figure 6. Seasonal variability in terminus area for each sector of Hubbard Glacier, normalized per year (1972–2013). Solid lines show the fourth-order polynomial fit to the data.

Inflection in the curves of regions A and B (Figure 5) in 1988 and 2006 likely reflect the migration of the medial moraine to its presurge position.

Ice draining into Russell Fiord (Region D) is advancing faster than any other region, at ~50 m yr^{-1} since 1984. Water depths in Russell Fiord are about a seventh of those in Disenchantment Bay, which likely explains this larger advance rate. Region D also undergoes a large seasonal variability in terminus position, with longer-term advance/retreat cycles occurring at ~7 year intervals, consistent with observations by *Ritchie et al.* [2008].

To investigate the seasonal patterns in terminus area observed in Figure 5, we normalize the area for each year and stack the results (Figure 6). Years with four or fewer area measurements are not included. The pattern of seasonal variability in terminus position is, in general, similar to other tidewater glacier systems in Alaska [e.g., *Krimmel*, 2001] and Greenland [e.g., *Schild and Hamilton*, 2013]. Annual advance begins in late February/early March (0.2 decimal years in Figure 6), peaks in May/June (0.45 decimal years), and reaches a minimum in November through January. This pattern is more clearly defined in Regions C and D, which could be due to the fact that Regions A and B share a medial moraine that is not fixed between epochs thereby making some of the area change attributable to moraine migration. *McNabb and Hock* [2014] observe a similar pattern of seasonal front positions across the whole terminus.

3.2. Ice Velocity

Large-scale ice flow patterns are primarily controlled by Hubbard Glacier's unique geometry. The general pattern of the Landsat-derived flowfield (Figure 3) is consistent with point measurements made using photogrammetry from 1978 to 1997 [*Trabant et al.*, 2003] and 2002 [*Motyka and Truffer*, 2007]. Velocities derived from the feature tracking method are also within 5% of the GPS velocities, despite the different sampling epochs. Figure 7 shows centerline flow speeds along the profile in Figure 3. The centerline velocity highlights several along-flow speed increases, caused by glacier narrowing (x = 0–5 km), glacier steepening (x = 14–16 km), seasonal changes in basal friction, and the influx of ice from Valerie Glacier to the west (x = 20–26 km) (Figure 7). The abrupt widening as the trunk enters the overdeepened terminal lobe results in a marked slow-down at x =16 km [*Trabant et al.*, 1991, 2003]. In the absence of digitized bed topography data we cannot compare ice flux values and thus focus on ice velocity comparisons.

Any long-term ice velocity trend is difficult to isolate from seasonal variability, due to the scarcity of velocity measurements (Figure 8). Since flow speeds can vary seasonally from 1500 to 5200 m yr^{-1} (see Figure 7),

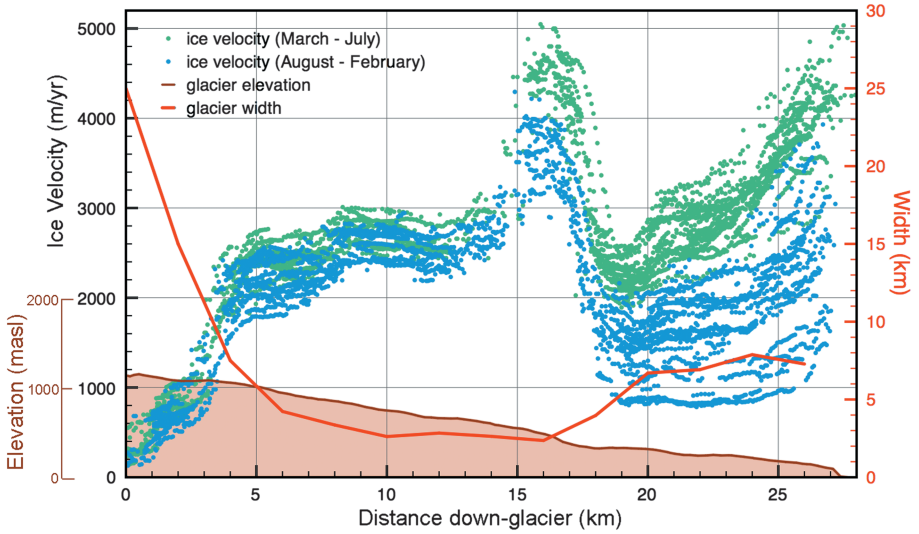

Figure 7. Ice velocity for every epoch, grouped from March to July (green) and August to February (blue), for the centerline profile displayed in Figure 3. Seasonal grouping is based on results of velocity minima and maxima shown in Figure 9. Surface elevation (brown) and glacier width (red) are derived along the same centerline profile.

nearly continuous measurements of ice velocity over the past few decades would be necessary to determine the existence of a long-term velocity trend. As a result, we focus primarily on seasonal variability, which is not uniform across the terminus. We stack the velocity data from 1985 to 2011 to isolate how different terminus regions vary seasonally (Figure 9). Winter velocities are averaged using fall to spring observations as illustrated by the width of the bars in Figures 8 and 9. Although there is interannual variability, the general pattern for regions B, C, and D is ice velocity reaching a maximum in April/May and a minimum in October/November. This seasonality in ice flow is similar to that on Columbia Glacier, AK (located 430 km to the northeast of Hubbard) which, in the early portion of its rapid retreat, reached a velocity peak in March and a minimum in September [*Krimmel*, 2001]. Region A, which drains from Valerie Glacier, reaches its maximum speed in July/August. Figure 9 also shows that ice velocity is not necessarily anomalous during years when there are ice or sediment dams at Gilbert Point. Across all regions of the terminus lobe, ice velocity in 1986 and 2002 is comparable to other years.

Overall, the seasonal strain rates of Hubbard Glacier are typical of Alaskan tidewater glaciers [e.g., *Marshall et al.*, 2002; *O'Neel and Pfeffer*, 2005]. Figure 10 shows a typical example for spring, when nominal strain rate amplitudes peak simultaneous with flow acceleration and terminus advance. Patterns of extension ($\dot{\varepsilon}'_{xx} > 0$, $\dot{\varepsilon}'_{yy} > 0$) dominate the terminal lobe, except at the glacier front where compression rates are high. All strain rate components, including compression at the terminus, diminish throughout the summer as the glacier decelerates and retreats (Figure 10, bottom). The strain rates in Figure 10 are typical of spring and fall patterns calculated throughout the record.

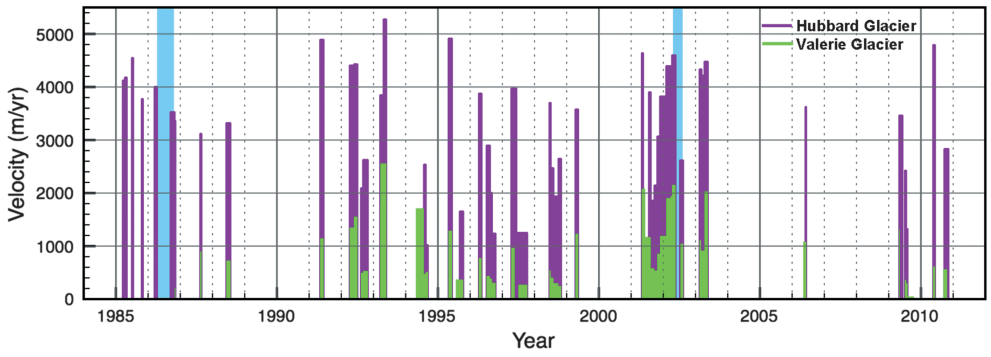

Figure 8. Ice velocities at the terminus of Hubbard Glacier (purple) and Valerie Glacier (green) where it merges with Hubbard Glacier. The width of the bars represents the time separation of images used to derive ice velocity. Blue bars indicate time periods when the terminus reached Gilbert Point.

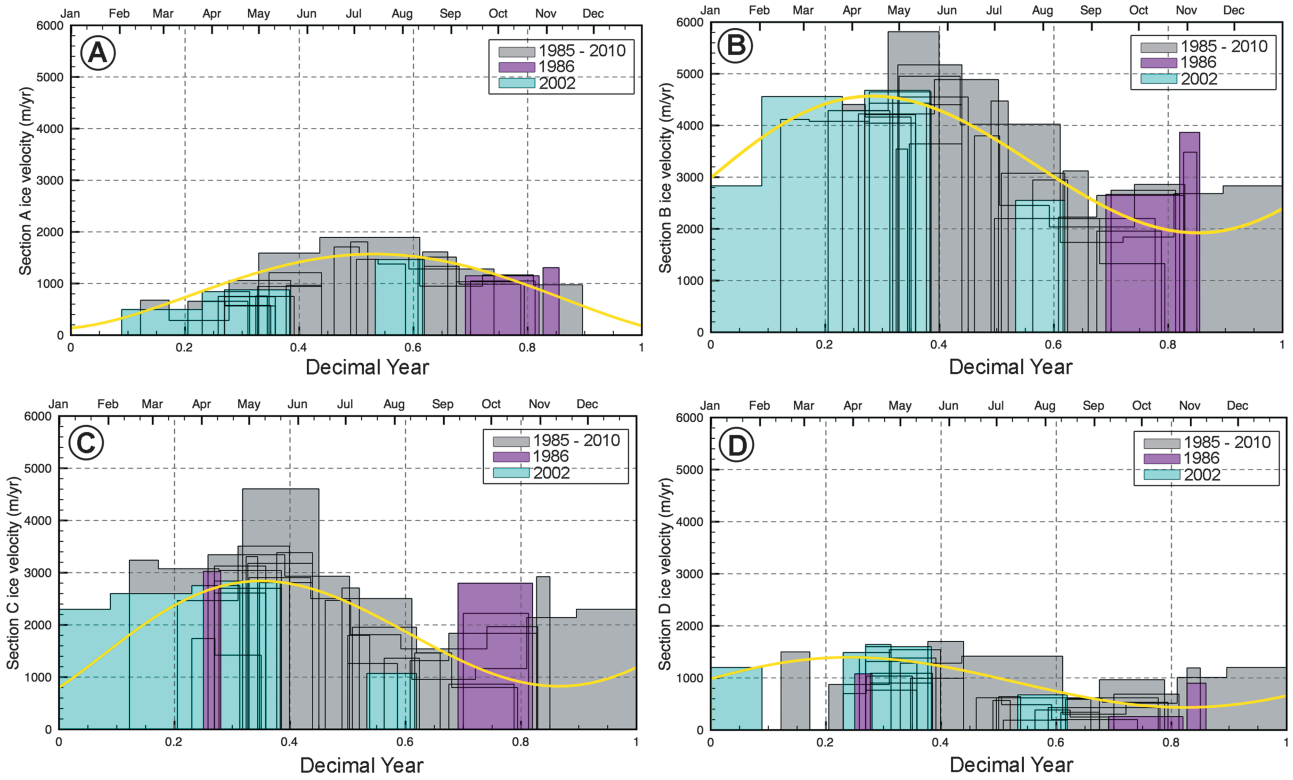

Figure 9. Ice velocity measurements at the terminus of Hubbard Glacier, from 1985 to 2010, separated by region (Figure 2). The width of the bars denotes the time separation between images used to derive velocities. Velocities from all years (except 1986 and 2002) are in grey; closure years 1986 and 2002 are in magenta and blue, respectively. The yellow line is a fourth-order polynomial fit to the velocity data.

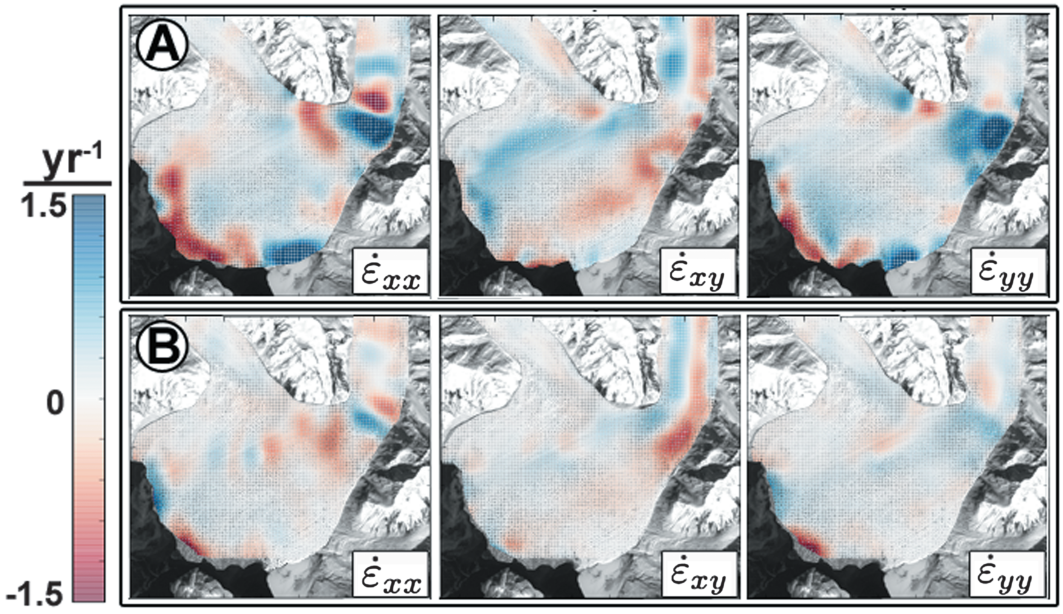

Figure 10. Strain rate components for a typical (a) spring and (b) fall overlain on a Landsat ETM+ image from 24 April 2002 [*NASA Landsat Program*, 2002]. Strain components are longitudinal strain rate ($\dot{\varepsilon}'_{xx}$), shear strain rate ($\dot{\varepsilon}'_{xy}$), and lateral strain rate ($\dot{\varepsilon}'_{yy}$). Positive values are extensional, negative values are compressional. Strain rates are flow following, where x is along flow and y is across flow. The strain rates were calculated using velocity data from 10 March to 11 April 2003 (with an average strain rate error of 0.23 year^{-1}), and August to September 1994 (with an average strain rate error of 0.59 year^{-1}).

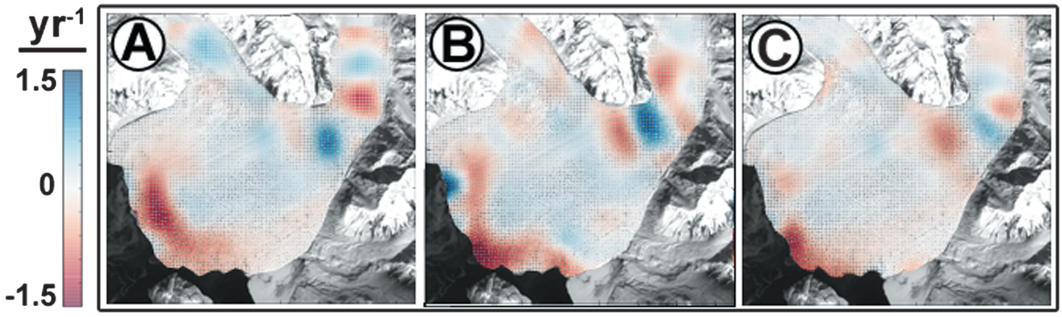

Figure 11. Longitudinal strain rates ($\dot{\varepsilon}_{xx}$) calculated using velocity data from (a) 3 February to 23 March 2002 (with an average strain rate error of 0.14 year^{-1}); (b) 23 March to 24 April 2002 (with an average strain rate error of 0.23 year^{-1}); (c) 13 July to 14 August 2002 (with an average strain rate error of 0.23 year^{-1}). The results are overlain on a Landsat ETM+ image from 24 April 2002 [*NASA Landsat Program*, 2002].

In comparison, strain rates before and during the 2002 closure event show unique changes in compression at the terminus (Figure 11). In February–March 2002 longitudinal compression is similar to other nonclosure years (Figure 10), exhibiting an extensive compressional band across the whole terminus. Usually, this compression reduces as the terminus retreats off the terminal moraine later in the summer. Figure 11 shows that longitudinal compression intensifies at Gilbert Point throughout 2002, from February until early August, coincident with the accumulation of sediment west of Gilbert Point.

The sediment dam that blocked the channel between Russell Fiord and Disenchantment Bay was located directly west of Gilbert Point [*Motyka and Truffer*, 2007]. Proglacial sediments were visible in front of the glacier terminus in aerial photographs taken on 2 May 2002 [*Motyka and Truffer*, 2007]. The growing moraine effectively shut down ice calving and narrowed the channel until it was completely closed off in mid-June—at this time the moraine was 5 m above sea level and 50 m wide [*Motyka and Truffer*, 2007]. The sediment dam was breached on 14 August [*Motyka and Truffer*, 2007]; unfortunately, we could not derive velocities using the feature tracking method during the fall or winter of 2002 due to a lack of available imagery.

3.3. Climate

Climate indices from 1970 to 2014 reveal a high degree of variability (Figure 12), but none that appears to directly control the terminus position. Terminus area does not appear to be influenced by seasonal extremes in air and ocean surface temperature, or PDO phase. There does appear to be a weak correlation between increased precipitation rates and terminus advance, particularly between 1984 and 1995. The role of the PDO index on these environmental variables in Alaska is debated [e.g., *McAfee*, 2014], and we do not observe a clear relationship between PDO phase and air temperature or precipitation as seen in other coastal stations [*Arendt et al.*, 2009] or high elevation sites [*Foy et al.*, 2011]. The PDO index is derived from monthly sea surface temperature variability in the North Pacific, so the correlation with local sea surface temperature is not surprising.

4. Discussion

4.1. Terminus Advance

The terminus of Hubbard Glacier has advanced at a fairly constant rate over the past 40 years, but extending the record back to 1895 shows that advance rates can be variable on longer timescales (Figure 4). These shifts in advance rates can be due to variations in fjord depth as the glacier advances forward or shifts in climate parameters that impact ice flux, submarine melt rates, or calving.

As a first step toward understanding variability in advance rates, we investigate the importance of air temperature, precipitation, and ocean temperature in modulating terminus area throughout the past 43 years (Figure 12). We compare the raw values of each of these parameters and also calculate variable anomalies with respect to the average annual cycle (Figure 12). To explore links between climate oscillations and terminus area change, we perform a power-spectrum analysis of the raw data in Figure 12. The only common frequency detected through this analysis is the strong annual cycle. Air and ocean temperatures and precipitation rates have a secondary peak at 11 years, which is not observed in the terminus area change. Additionally, closure events do not ubiquitously coincide with distinct climate anomalies (Figure 12).

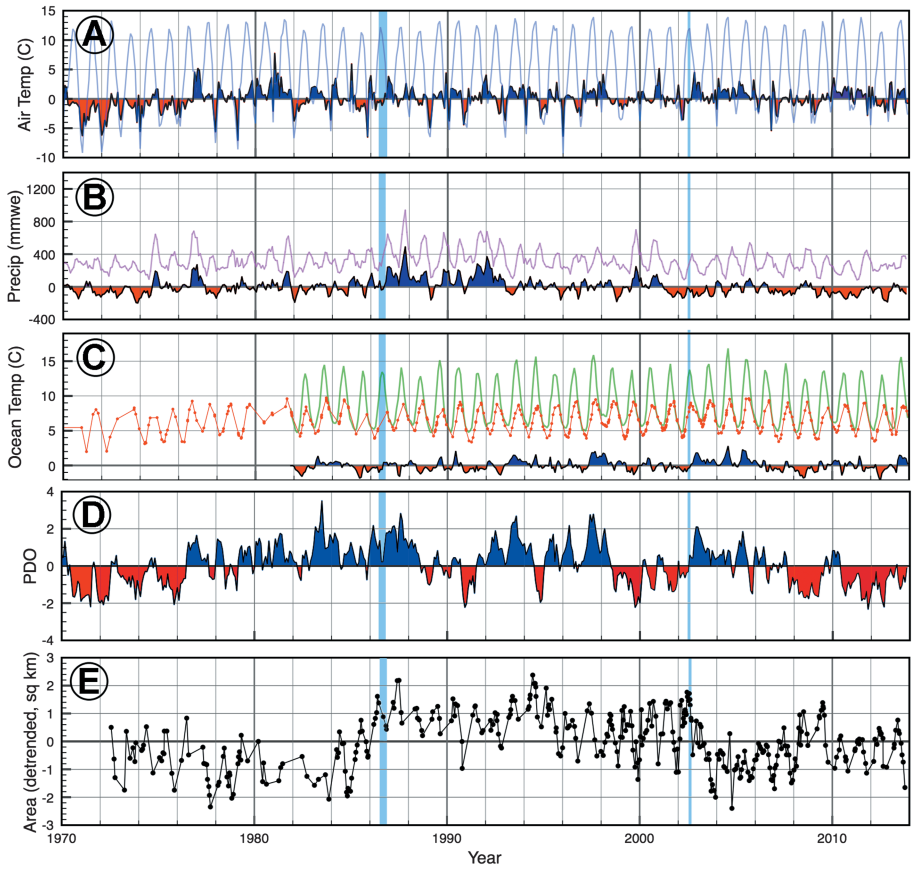

Figure 12. Monthly climate indices (colored lines) and anomalies from the average annual cycle (black, with red and blue shading). (a) Air temperature from Yakutat station (WMO station: 70361) in °C. (b) Precipitation from Yakutat station (WMO station: 70361) in millimeters water equivalent. (c) Sea surface temperatures (green) and anomalies reconstructed for an area including all of Disenchantment Bay (°C). Alaskan Current temperatures (red) from a station near Seward (°C). (d) Pacific Decadal Oscillation Index. (e) Total area of Hubbard terminus (as seen in Figure 5a), detrended. Blue bars indicate time periods when the terminus reached Gilbert Point.

Hubbard Glacier's rate of advance has been fairly consistent since 1961, with the exception of a slower advance between 1972 (or earlier) and 1984 (Figures 5 and 12). We are unable to constrain when this slower advance rate began due to a lack of imagery between 1961 and 1972. A slower rate of advance could be due to a decrease in ice velocity (supplying less ice to the terminus), an increase in calving or submarine melt rate (removing more ice from the terminus), a deepening in the fjord bathymetry (requiring ice to thicken or sediment to accumulate in order to stabilize the advance), or a combination of these processes. Our results in Figure 12 do not show a clear correlation between any climate variable and this period of slower advance.

In contrast, the accelerated rate of terminus advance beginning in 1984 coincides with a period of increased precipitation rates. Higher precipitation rates likely lead to enhanced subglacial discharge, which could impact ice velocity and also subglacial sediment transport. However, increased subglacial discharge can also increase submarine melting [e.g., *Motyka et al.*, 2003], complicating the relationship between terminus position and precipitation. In addition, periods with comparatively low precipitation rates (e.g., 2001–2014) do not necessarily correspond with periods of slowed terminus advance. These results highlight the complexity of terminus dynamics and suggest that no single climate-related mechanism controls Hubbard Glacier's pattern of advance.

4.2. Seasonal Variations

Like many temperate glaciers, Hubbard Glacier exhibits strong seasonal variability both in terminus position (Figure 6) and ice velocity (Figure 9). Meltwater production in the spring overpressurizes the subglacial drainage system causing increased basal motion [e.g., *Iken and Truffer*, 1997]. As meltwater input continues, a more efficient subglacial hydrologic network reduces basal water pressure and the glacier decelerates [e.g.,

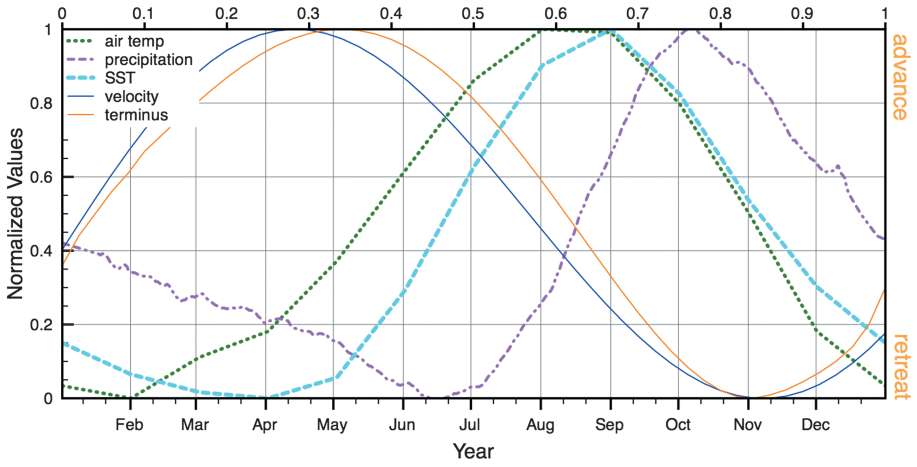

Figure 13. Patterns of seasonality for glacier behavior (ice velocity, terminus position) and environmental controls (sea surface temperature, air temperature) in and near Yakutat Bay. Terminus position (Figure 6b) and ice velocity (Figure 9b) for Region B is used because it is most representative of the terminus lobe. The values are normalized to highlight potential relationships.

Schoof, 2010; *Sundal et al.*, 2011; *Burgess et al.*, 2013]. The seasonal position of the terminus depends on several variables, including ice velocity, ice thickness, submarine melt rates, and bathymetry. A maximum terminus position is reached in May/June and a minimum in November/December. Of the 36 Alaskan tidewater glaciers analyzed by *McNabb and Hock* [2014], 23 of them show a similar seasonal advance/retreat cycle.

The seasonal timing of maximum advance and retreat is roughly consistent across the terminus and over the past 30 years (Figure 5) [*Ritchie et al.*, 2008]. Figure 13 shows the seasonal behavior of parameters that can modulate terminus position, which includes atmospheric and oceanic forcings [*Straneo et al.*, 2013]. Enhanced surface melting can propagate to the bed and increase the sliding speed [e.g., *Kamb*, 1987]; changes in submarine melt rates can alter the calving rate and thus the terminus position [*Motyka et al.*, 2003]. Submarine melt rates are a function of both the temperature of incoming fjord water and subglacial freshwater discharge [*Motyka et al.*, 2013]. Upwelling of fresh water along the calving face drives convection of relatively warm ocean water such that increased subglacial discharge and warm ocean temperatures in the summer result in high rates of submarine melting [*Motyka et al.*, 2003]. The impact that ocean temperatures have on submarine melt rates can be large. *Motyka and Truffer* [2007] estimate a threefold seasonal increase in submarine erosion rates based on observations of a 7°C temperature fluctuation in Disenchantment Bay between early spring and late summer.

Figure 13 shows a correlation, with slight lag, between maximum ice velocity and terminus position, both of which precede the maximum in air and sea surface temperature. This plot shows the sensitivity of ice velocity to spring warming and the importance of ice velocity in controlling the terminus position. The terminus advances with the increase in ice velocity and when ocean temperatures are cool, which would reduce submarine melt rates. Interestingly, the terminus continues to advance after the velocity maximum, beginning its retreat only when ocean temperatures start to increase in May. Sea surface temperatures (SSTs) closely follow air temperatures; precipitation values are highest in the winter and lowest in the early summer; thus, the precipitation likely falls as snow and may fuel the following season's advance [*Burgess et al.*, 2013].

We further investigate the relationship between ice velocity and terminus position by calculating the calving rate ($\dot{c}$), which is the difference between ice velocity at the front margin (u_M) and the rate of change in the position of the calving face (L), as prescribed by

$$\dot{c} = u_M - \frac{dL}{dt}. \tag{2}$$

It should be noted that the term "calving rate" as used here refers to both iceberg calving and submarine melting (also referred to as frontal ablation); the position of the calving face is impacted by both of these processes and the individual impacts cannot easily be separated. As with most well-grounded, advancing glaciers, calved icebergs are generally small and submarine melting likely dominates terminus loss on Hubbard Glacier. The relative importance of each of the terms in equation (2) varies seasonally and across the terminus, as

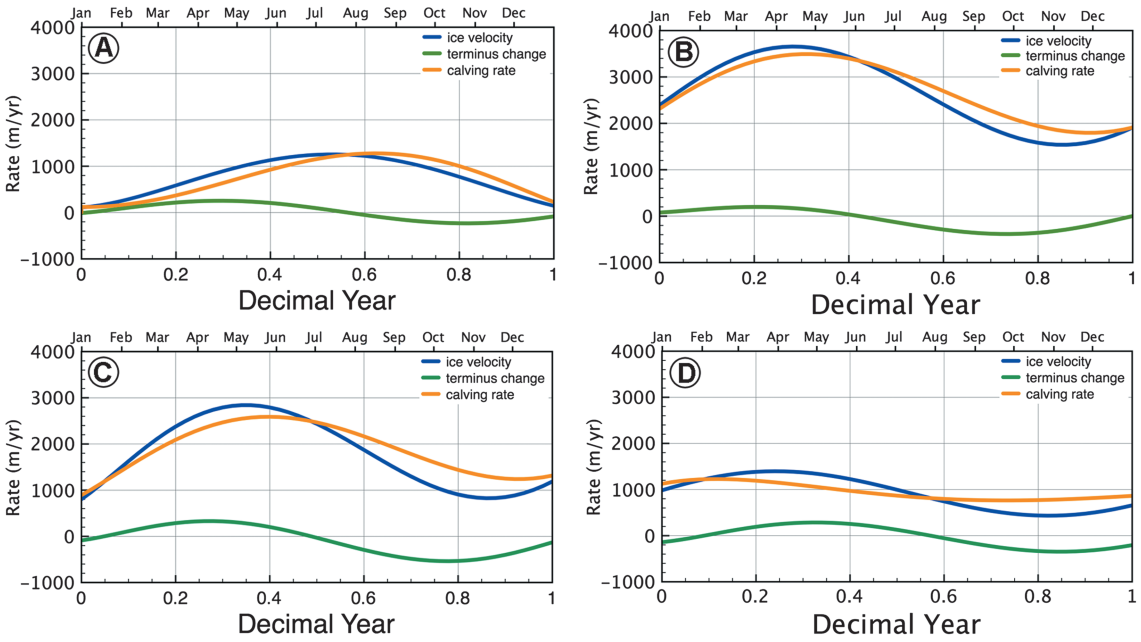

Figure 14. Calving rate estimates for Regions A–D of the terminus.

shown in Figure 14. We determine the calving rate across each region of the terminus (see Figure 2) using the curve fits for terminus change and ice velocity shown in Figures 6 and 9. Ice velocity values are scaled to reflect the width-averaged velocity of each terminus region.

Figure 14 shows that the calving rate is closely correlated with ice flow but is also likely influenced from factors including proximity to the terminal moraine and changes in submarine melting. Velocity increases in early spring as does the calving rate. When the calving rate is less than the ice velocity, the terminus advances. The terminus reaches a maximum position in May/June, at which point the calving rate exceeds the ice velocity and the terminus starts to retreat. Retreat continues until November/December when ice velocity slowly increases and the terminus again advances. This pattern is fairly uniform across the margin, with the exception of Region D. For unknown reasons, the area that drains into Russell Fiord has a high calving rate early in the year (January/February), which slowly (and nearly linearly) decreases throughout the rest of the year (Figure 14d).

Submarine melting is an important component of terminus loss on tidewater glaciers in Alaska [e.g., *Motyka et al.*, 2003; *Ritchie et al.*, 2008; *Bartholomaus et al.*, 2013] and can be enhanced by warmer ocean temperatures, more vigorous ocean currents, and increases in subglacial discharge. *Motyka and Truffer* [2007] use estimates of water temperature and velocity at Gilbert Point to calculate submarine melt rates. They conclude that melt rates result in a change in terminus position ranging from 475 to 1643 m yr^{-1}, depending on water temperatures. For ice adjacent to Gilbert Point (Figure 14c), submarine melting would thus account for nearly all of the mass loss and iceberg calving is likely minimal. While water velocities are slower outside of the Gilbert Point gap, submarine melting likely remains an important component of terminus loss and undercutting.

4.3. Terminus Closure at Gilbert Point

Of particular societal interest is the probable transformation of Russell Fiord into Russell Lake. Given the steady advance (~35 m yr^{-1}) of the terminus and the high AAR (0.95) of Hubbard Glacier it is unlikely that the channel between Russell Fiord and Disenchantment Bay will remain open throughout this century. Additional processes that could trigger closure include ice acceleration (of Hubbard or Valerie glaciers), an increase in subglacial sediment supply, or a decrease in submarine melt rates [*Motyka and Truffer*, 2007; *Ritchie et al.*, 2008].

While ice velocity strongly impacts the terminus position (Figure 14), it does not appear to control individual closure events (Figures 8 and 9). The magnitude of ice velocity before and during closure years is not different from the magnitude in intervening years. This is true for both Hubbard and Valerie glaciers. We see no evidence

that the 1986 closure was caused by a coincident surge of Valerie Glacier, as proposed by *Mayo* [1989]. In fact, the medial moraine began to shift toward the Hubbard lobe in 1984—two years before the surge of Valerie Glacier and the closure at Gilbert Point.

Ice velocity patterns, not magnitude, do appear to play an important role in closure events [*Motyka and Truffer*, 2007]. Large compressional strain rates at the terminus coincide with the emergence of a narrow shoal directly west of Gilbert Point (Figure 11). The 1986 closure occurred in a similar area, although sediment was not visible above the water line [*Trabant et al.*, 1991]. The moraine grows in a narrow region where the fjord is shallow, and water velocities are reduced. The fjord rapidly deepens toward Disenchantment Bay to the west (Figure 2), and high water velocities in the narrow gap likely reduce sediment accumulation and terminus advance [*Motyka and Truffer*, 2007]. The rapid growth of the moraine during closure years suggests that sedimentation rates at Hubbard Glacier are high. While the mechanism that causes occasional sediment routing toward Gilbert Point remains unknown, subglacial processes are clearly dynamic.

The temporary closures in 1986 and 2002 did coincide with temporal maxima in the total terminus area; however, these local maxima were driven by the combined contribution of Regions A, C, and D (Figure 5). Region B (Hubbard Glacier ice that drains into Disenchantment Bay) did not advance in years preceding closure events (Figure 5). This observation suggests that Valerie Glacier may still contribute to the closures at Gilbert Point, despite a lack of evidence linking closures to surge events. It is possible that changes in flow patterns between Valerie and Hubbard glaciers led to rerouting of basal water and sediments, which could trigger closure events [*Ritchie et al.*, 2008].

4.4. Role of Terminal Moraine

An important control on tidewater glacier terminus position is the growth and location of the submarine moraine [*Powell*, 1991]. Studies of paleomoraines suggest that an ice face and morainal bank move as the combined result of ice shoving and internal deformation of the moraine [e.g., *Boulton*, 1986; *Motyka et al.*, 2006]. The importance of sediment accumulation at the grounding line in maintaining glacier stability has been discussed in other fjord and shelf settings [e.g., *Powell*, 1991; *Alley et al.*, 2007; *Benn et al.*, 2007; *Nick et al.*, 2007] and likely plays an important role in the seasonal and long-term terminus position of Hubbard Glacier.

The geometry and location of the moraine is known from repeat bathymetric surveys made in 1977 [*NOAA*, 1984], 1986 [*Mayo*, 1989], 1999 [*NOAA*, 2000], 2002, 2004 [*Motyka and Truffer*, 2007], and 2008 [*Finnegan et al.*, 2010] (see Figure 2). These surveys show a general migration of the morainal bank and that the moraine geometry is quite variable over short timescales [*Goff et al.*, 2012]. The seafloor is shallow (−25 m) and smooth in the Gilbert Point gap with a pronounced erosional channel ∼5 km west and substantially deeper water in Disenchantment Bay (Figure 2). Erosional and depositional features modify the fjord depths substantially in the intervening years. Reports of moraine height vary from ∼20 m immediately to the west of Gilbert Point [*Finnegan et al.*, 2010; *Goff et al.*, 2012] where closure occurred in both 1986 and 2002, to 50–85 m in Disenchantment Bay and Russell Fiord [*NOAA*, 2000; *Trabant et al.*, 2003; *Motyka and Truffer*, 2007; *Goff et al.*, 2012].

A recent study by *Goff et al.* [2012] describes the migration of the morainal bank in front of Hubbard Glacier from repeat bathymetric surveys in 1978, 1999, and 2010. Between 1978 and 2010, the morainal bank moved at an average rate of ∼32 m yr^{-1}; during this time the terminus (Region B) advanced by 33 m yr^{-1} (similar to findings by *Trabant et al.* [2003]). Interestingly, *Goff et al.* [2012] also found that sedimentation rates increased from $\sim 0.88 \pm 0.03$ m yr^{-1} between 1978 and 1999 to $\sim 1.22 \pm 0.01$ m yr^{-1} between 1999 and 2010—consistent with our findings for terminus Region B (Figure 5) showing an increase in advance rate over the last decade.

The presence and mobility of Hubbard Glacier's terminal moraine is an important component of its advance. Variations in moraine height and mobility likely cause the different advance/retreat patterns observed across the terminal lobe (Figure 5). The height of the moraine increases into Disenchantment Bay (Figure 2), providing a stable foundation for terminus advance [*Goff et al.*, 2012]. Water depths extending into Russell Fiord remain shallow and we therefore expect sustained high rates of advance into Russell Fiord in the future. Shallow water also exists at the Gilbert Point gap, but advance rates are minimal suggesting that submarine melt rates are high. Submarine melt rates are governed by water temperature and velocity, and as the gap narrows, tidal currents increase in speed. However, the likelihood of permanent closure increases as the terminus continues to wrap around Gilbert Point.

5. Conclusions

Hubbard Glacier's terminus position is controlled by a combination of atmospheric, oceanographic, and glaciological forcings. The terminus advances because of the glacier's high accumulation-to-area ratio (AAR) and steadily growing terminal moraine. This long-term trend is likely modulated, at the decadal scale, by moraine geometry and submarine melt rates. Ice velocity and regional climate forcings do not appear to cause decadal variations in terminus position, although the noncontinuous ice velocity record prevents subannual analysis. Ice velocity variability does drive seasonal advance/retreat cycles at the terminus. Both velocity and terminus position reach a maximum in early spring and a minimum in winter.

Temporary closure events can be driven by short-term perturbations that impact moraine properties or the calving rate at, or adjacent to, Gilbert Point. Forcings that cause ice velocity acceleration (anomalous precipitation events or a surge of Valerie Glacier), reduce calving (decrease in submarine melting), or change the geometry of the moraine (increase in sediment supply or change in sediment routing) will further increase advance rates across the terminus. Sustained closure will occur by 2045 if the terminus adjacent to Gilbert Point continues to advance at its current rate (13 m yr^{-1}); if the terminus advances at its width-averaged rate, closure will occur by 2025. These closures will likely persist unless climate warms enough to raise the ELA by 1000 m, thereby lowering the AAR enough to stop terminus advance or sediment supply to the morainal bank is reduced.

Acknowledgments

The supporting information list images used in this study to derive terminus area and ice velocity. Ice velocity and terminus data products are available on the CRREL glacier data repository: www.glacierresearch.org/locations/hubbard/satellite-data. This work was partially funded by an NSF RAPID grant awarded to D. Lawson (NSF-OPP/ARC-094977). The authors would also like to thank the community of Yakutat and the US Army Corps of Engineers-Alaska District, Anchorage, Alaska. We thank Martin Truffer, Roman Motyka, and Jeremy Bassis for providing insightful edits that greatly improved this manuscript.

References

Alley, R., S. Anandakrishnan, T. Dupont, B. Parizek, and D. Pollard (2007), Effect of sedimentation on ice-sheet grounding-line stability, *Science*, *315*(5820), 1838–1843.

Arendt, A., K. Echlemeyer, W. Harrison, C. Lingle, S. Zimheld, V. Valentine, B. Ritchie, and M. Druckenmiller (2006), Updated estimates of glacier volume changes in the western Chugach Mountains, Alaska, and a comparison of regional extrapolation methods, *J. Geophys. Res.*, *111*, F03019, doi:10.1029/2005JF000436.

Arendt, A., J. Walsh, and W. Harrison (2009), Changes of glaciers and climate in northwestern north America during the late twentieth century, *J. Clim.*, *22*, 4117–4134.

Barclay, D., P. Calkin, and G. Wiles (2001), Holocene history of Hubbard Glacier in Yakutat Bay and Russell Fiord, southern Alaska, *Geol. Soc. Am. Bull.*, *113*(3), 388–402.

Bartholomaus, T., C. Larsen, and S. O'Neel (2013), Does calving matter? Evidence for significant submarine melt, *Earth Planet. Sci. Lett.*, *380*, 21–30, doi:10.1016/j.epsl.2013.08.014.

Benn, D., C. Warren, and R. Mottram (2007), Calving processes and the dynamics of calving glaciers, *Earth Sci. Rev.*, *82*(3-4), 143–179, doi:10.1016/j.earscirev.2007.02.002.

Boulton, G. S. (1986), Push moraines and glacier-contact fans in marine and terrestrial environments, *Sedimentology*, *33*(5), 677–698.

Burgess, E. W., C. Larsen, and R. R. Forster (2013), Summer melt regulates winter glacier flow speeds throughout Alaska, *Geophys. Res. Lett.*, *40*, 6160–6164, doi:10.1002/2013GL058228.

Daly, S. F., C. Vouyovich, and D. C. Finnegan (2011), Situk River Hydrology Following Closure of Russell Fiord by Hubbard Glacier, *ERDC-CRREL Tech. Rep. ADA53802*, Cold Regions Research and Engineering Laboratory, Hanover, N. H.

Finnegan, D. C., D. E. Lawson, W. Butler, and T. Waller (2010), Multibeam bathymetry, terrestrial LiDAR topography and three-dimensional velocity structure observations of the ice marginal marine environment, Hubbard Glacier, Alaska, *ERDC-CRREL Tech. Rep. 10-08*, Cold Regions Research and Engineering Laboratory, Hanover, N. H.

Foy, N., L. Copland, C. M. Zdanowicz, M. N. Demuth, and C. Hopkinson (2011), Recent volume and area changes of Kaskawulsh Glacier, Yukon Canada, *J. Glaciol.*, *57*, 515–525.

Goff, J. A., D. E. Lawson, B. A. Willems, M. Davis, and S. P. S. Gulick (2012), Morainal bank progradation and sediment accumulation in Disenchantment Bay, Alaska: Response to advancing Hubbard Glacier, *J. Geophys. Res.*, *117*, F02031, doi:10.1029/2011JF002312.

Iken, A., and M. Truffer (1997), The relationship between subglacial water pressure and velocity of Findelengletscher, Switzerland, during its advance and retreat, *J. Glaciol.*, *43*(144), 328–338.

Jaeger, J. C., and N. Cook (1976), *Fundamentals of Rock Mechanics*, Halsted Press, New York.

Kamb, B. (1987), Glacier surge mechanism based on linked cavity configuration of the basal water conduit system, *J. Geophys. Res.*, *92*(B9), 9083–9100, doi:10.1029/JB092iB09p09083.

Krimmel, R. M., (2001), Photogrammetric data set, 1957–2000, and bathymetric measurements for Columbia Glacier, Alaska, *Tech. Rep. 01-4089*, U.S. Geological Survey - Water Resources Investigations Report, Reston, Va. [Available at http://pubs.usgs.gov/wri/wri014089/.]

Krimmel, R. M., and W. Sikonia (1986), Velocity and surface altitude of the lower part of Hubbard Glacier, Alaska, 1978, Department of the Interior, *U.S. Geol. Surv. Open File Rep.*, 86–549.

Larsen, C., R. J. Motyka, A. Arendt, and K. A. Echelmeyer (2007), Glacier changes in southeast Alaska and northwest British Columbia and contribution to sea level rise, *J. Geophys. Res.*, *112*, F01007, doi:10.1029/2006JF000586.

Lichten, S. M., and J. S. Border (1987), Strategies for high-precision Global Positioning System orbit determination, *J. Geophys. Res.*, *92*, 12,751–12,762, doi:10.1029/JB092iB12p12751.

Marshall, H. P., J. T. Harper, W. T. Pfeffer, and N. F. Humphrey (2002), Depth-varying constitutive properties observed in an isothermal glacier, *Geophys. Res. Lett.*, *29*(23), 2146, doi:10.1029/2002GL015412.

Mayo, L. R. (1989), Advance of Hubbard Glacier and 1986 outburst of Russell Fiord, Alaska, USA, *Ann. Glaciol.*, *13*, 189–194.

McAfee, S. A. (2014), Consistency and the lack thereof in Pacific Decadal Oscillation impacts on North American winter climate, *J. Clim.*, *27*, 7410–7431.

McNabb, R. W., and R. Hock (2014), Alaska tidewater glacier terminus positions, 1948–2012, *J. Geophys. Res. Earth Surf.*, *119*, 153–167, doi:10.1002/2013JF002915.

Meier, M., M. Dyurgerov, U. Rick, S. O'Neel, W. Pfeffer, R. Anderson, S. Anderson, and A. Glazovsky (2007), Glaciers dominate eustatic sea-level rise in the 21st century, *Science*, *317*(5841), 1064–1067, doi:10.1126/science.1143906.

Moon, T., and I. Joughin (2008), Changes in ice front position on Greenland's outlet glaciers from 1992 to 2007, *J. Geophys. Res.*, *113*, F02022, doi:10.1029/2007JF000927.

Motyka, R., and M. Truffer (2007), Hubbard Glacier, Alaska: 2002 closure and outburst of Russell Fjord and postflood conditions at Gilbert Point, *J. Geophys. Res.*, *112*, F02004, doi:10.1029/2006JF000475.

Motyka, R. J., L. Hunter, K. A. Echelmeyer, and C. Connor (2003), Submarine melting at the terminus of a temperate tidewater glacier, LeConte Glacier, Alaska, USA, *Ann. Glaciol.*, *36*(1), 57–65.

Motyka, R. J., M. Truffer, E. M. Kuriger, and A. K. Bucki (2006), Rapid erosion of soft sediments by tidewater glacier advance: Taku Glacier, Alaska, USA, *Geophys. Res. Lett.*, *33*, L24504, doi:10.1029/2006GL028467.

Motyka, R. J., W. P. Dryer, J. Amundson, M. Truffer, and M. Fahnestock (2013), Rapid submarine melting driven by subglacial discharge, LeConte Glacier, Alaska, *Geophys. Res. Lett.*, *40*, 5153–5158, doi:10.1002/grl.51011.

NASA Landsat Program (2002), *Landsat ETM+, SLC Off*, scene L71062018-01820020424, 04/24/2002, USGS, Sioux Falls, S. D.

NASA Landsat Program (2003), *Landsat ETM+, SLC Off*, scene L71062018-01820030809, 08/09/2003, USGS, Sioux Falls, S. D.

Nick, F. M., C. J. van Der Veen, and J. Oerlemans (2007), Controls on advance of tidewater glaciers: Results from numerical modeling applied to Columbia Glacier, *J. Geophys. Res.*, *112*, F03S24, doi:10.1029/2006JF000551.

NOAA (1984), Yakutat Bay, Alaska, in *Chart 16761*, pp. 13th ed., scale 1:80000, National Ocean Service, Silver Spring, Md.

NOAA (2000), Yakutat Bay, Alaska, in *Chart 16761*, pp. 16th ed., scale 1:80000, National Ocean Service, Silver Spring, Md.

O'Neel, S., and T. Pfeffer (2005), Evolving force balance at Columbia Glacier, Alaska, during its rapid retreat, *J. Geophys. Res.*, *110*, F03012, doi:10.1029/2005JF000292.

Post, A. (1975), *Preliminary Hydrology and Historic Terminal Changes of Columbia Glacier*, U.S. Geol. Surv. Hydrol. Invest. Atlas, Alaska.

Post, A., S. O'Neel, R. J. Motyka, and G. Streveler (2011), A complex relationship between calving glaciers and climate, *Eos Trans. AGU*, *92*(37), 305, doi:10.1029/2011EO370001.

Powell, R. D. (1991), Grounding-line systems as second-order controls on fluctuations of tidewater termini of temperate glaciers, in *Glacial Marine Sedimentation; Paleoclimatic Significance*, edited by J. B Anderson and G. M. Ashley, *Geol. Soc. Am. Spec. Pap.*, *261*, 75–93, doi:10.1130/SPE261-p75.

Rignot, E., J. Mouginot, C. Larsen, Gimm Y., and D. Kirchner (2013), Low-frequency radar sounding of temperate ice masses in Southern Alaska, *Geophys. Res. Lett.*, *40*, 5399–5405, doi:10.1002/2013GL057452.

Ritchie, J., C. Lingle, R. Motyka, and M. Truffer (2008), Seasonal fluctuations in the advance of a tidewater glacier and potential causes: Hubbard Glacier, Alaska, USA, *J. Glaciol.*, *54*(186), 401–411.

Scambos, T., M. Dutkiewicz, J. Wilson, and R. Bindschadler (1992), Application of image cross-correlation to the measurement of glacier velocity using satellite image data, *Remote Sens. Environ.*, *42*(3), 177–186.

Schild, K., and G. S. Hamilton (2013), Seasonal variations of outlet glacier terminus position in Greenland, *J. Glaciol.*, *59*(216), 759–770.

Schoof, C. (2010), Ice-sheet acceleration driven by melt supply variability, *Nature*, *468*(7325), 803–806, doi:10.1038/nature09618.

Stearns, L. A., and H. Jiskoot (2014), *Global Land Ice Measurements from Space (GLIMS)*, chap. Glacier fluctuations and dynamics around the margin of the Greenland Ice Sheet, Praxis-Springer, Berlin.

Straneo, F., et al. (2013), Challenges to understanding the dynamic response of Greenland's Marine terminating glaciers to oceanic and atmospheric forcing, *Bull. Am. Meteorol. Soc.*, *94*(8), 1131–1144.

Sundal, A. V., A. Shepherd, P. Nienow, E. Hanna, S. Palmer, and P. Huybrechts (2011), Melt-induced speed-up of Greenland ice sheet offset by efficient subglacial drainage, *Nature*, *469*(7331), 521–524, doi:10.1038/nature09740.

Trabant, D. C., R. M. Krimmel, and A. Post (1991), A preliminary forecast of the advance of Hubbard Glacier and its influence on Russell Fiord, Alaska, *Tech. Rep. 90-4172*, U.S. Geological Survey, Water Resources Investigations Report, Univ. of Michigan.

Trabant, D. C., R. K. Krimmel, K. A. Echelmeyer, S. L. Zirnheld, and D. H. Elsberg (2003), The slow advance of a calving glacier: Hubbard Glacier, Alaska, U.S.A., *Ann. Glaciol.*, *36*, 45–50.

USGS (2006), *Shuttle Radar Topography Mission*, 30 Arc Second (GTOPO30) Mosaic, February 2000 coverage, Global Land Cover Facility, Univ. of Maryland, College Park, Md.

Wright, F. F., (1972), Marine geology of Yakutat Bay, Alaska, *Tech. Rep. 800-B*, *U.S. Geol. Surv. Prof. Pap.*, College, Alaska.

Wuite, J. (2006), Spatial and temporal dynamics of three East Antarctic outlet glaciers and their floating ice tongues, PhD thesis, The Ohio State University.